NANO LETTERS

Letter

pubs.acs.org/NanoLett

In Situ TEM of Two-Phase Lithiation of Amorphous Silicon Nanospheres

Matthew T. McDowell,[†] Seok Woo Lee,[†] Justin T. Harris,[‡] Brian A. Korgel,[‡] Chongmin Wang,[§] William D. Nix,[†] and Yi Cui*[,†,∥]

[†]Department of Materials Science and Engineering, Stanford University, Stanford, California 94305, United States

[‡]Department of Chemical Engineering, Texas Materials Institute, Center for Nano- and Molecular Science and Technology, The University of Texas at Austin, Austin, Texas 78712, United States

[§]Environmental Molecular Sciences Laboratory, Pacific Northwest National Laboratory, Richland, Washington 99354, United States

[∥]Stanford Institute for Materials and Energy Sciences, SLAC National Accelerator Laboratory, 2575 Sand Hill Road, Menlo Park, California 94025, United States

Supporting Information

ABSTRACT: To utilize high-capacity Si anodes in next-generation Li-ion batteries, the physical and chemical transformations during the Li−Si reaction must be better understood. Here, in situ transmission electron microscopy is used to observe the lithiation/delithiation of amorphous Si nanospheres; amorphous Si is an important anode material that has been less studied than crystalline Si. Unexpectedly, the experiments reveal that the first lithiation occurs via a two-phase mechanism, which is contrary to previous understanding and has important consequences for mechanical stress evolution during lithiation. On the basis of kinetics measurements, this behavior is suggested to be due to the rate-limiting effect of Si−Si bond breaking. In addition, the results show that amorphous Si has more favorable kinetics and fracture behavior when reacting with Li than does crystalline Si, making it advantageous to use in battery electrodes. Amorphous spheres up to 870 nm in diameter do not fracture upon lithiation; this is much larger than the 150 nm critical fracture diameter previously identified for crystalline Si spheres.

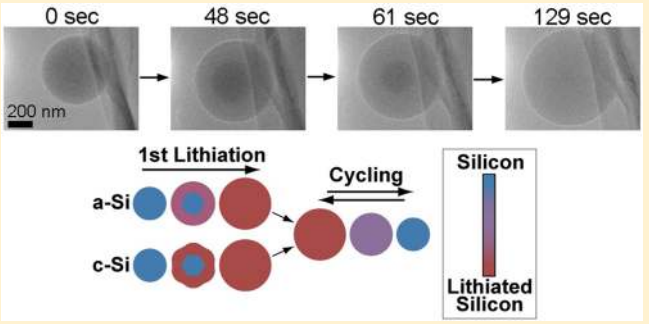

KEYWORDS: *Batteries, energy storage, phase transformations, silicon, in situ TEM*

Driven by emerging applications such as electric vehicles, there has been intense interest in recent years in developing new high-capacity materials for higher energy Li-ion batteries.[1−4] One such material, silicon, is an especially promising candidate for replacing the commercial graphite anode because its theoretical specific capacity is ten times higher than graphite.[5,6] However, problems resulting from the ∼300% volume expansion and contraction during lithium alloying/dealloying with silicon have prevented commercial implementation: these dimensional changes can result in fracture of active particles and unstable solid electrolyte interphase (SEI) growth, leading to loss of capacity with cycling.[6] Much progress has been made recently by designing silicon nanostructures that resist fracture or have dimensionally stable surfaces for SEI growth.[7−19] In parallel, these electrochemical studies have been guided by experiments using novel techniques to understand the Li−Si alloying reaction on the nanoscale.[20−35] In situ transmission electron microscopy (TEM) has been particularly useful and informative; in situ TEM studies have revealed important features of this reaction, including phase evolution,[26,36] anisotropic expansion and fracture behavior,[24] atomic level details of the lithiation of crystalline Si,[22] and the effect of stress on the kinetics of lithiation.[27] These studies have led to a more complete fundamental understanding of the lithiation process, but this research has focused primarily on the reaction process of crystalline Si (c-Si). In many cases, amorphous Si (a-Si) is used as the active material in battery electrodes; in addition, c-Si is converted to the amorphous phase and remains amorphous after the first cycle. As such, it is necessary to understand the volume expansion, lithiation dynamics, and stress evolution in a-Si particles to better engineer nanostructured a-Si anodes. Here, we present in situ TEM results showing the lithiation and delithiation of well-defined a-Si nanospheres. Interestingly, the a-Si spheres are lithiated by an unexpected mechanism that is similar to the two-phase reaction that occurs during lithiation of c-Si, but the kinetics of the reaction and fracture behavior are significantly different than in the crystalline case.

Received: December 3, 2012
Revised: January 3, 2013

dx.doi.org/10.1021/nl3044508 | *Nano Lett.* XXXX, XXX, XXX−XXX

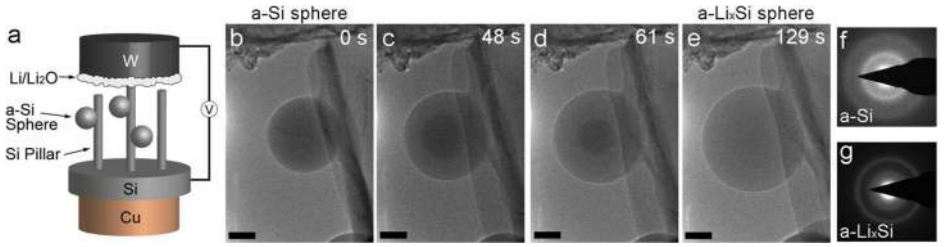

Figure 1. In situ experiments. (a) Schematic showing the in situ TEM cell. The a-Si spheres are dispersed onto c-Si pillar arrays etched into Si wafers, and the Si wafer is attached to a copper metal rod. The counter electrode (Li source) consists of Li metal with a thin Li_2O coating (solid electrolyte) on the tip of a tungsten rod. (b–e) Time series of the lithiation of a single a-Si sphere. The pillar to which the sphere is attached contacts the Li/Li_2O at the top of the frame, and both the pillar and the sphere are lithiated upon application of a bias. The relatively sharp contrast between the lithiated shell and the Si-rich core reveals an unexpected two-phase lithiation mechanism. The scale bars are 200 nm, and each image is labeled with the number of seconds after the first image was recorded. (f) Selected-area electron diffraction (SAED) pattern of a pristine a-Si sphere. (g) SAED pattern of a lithiated sphere showing its amorphous character.

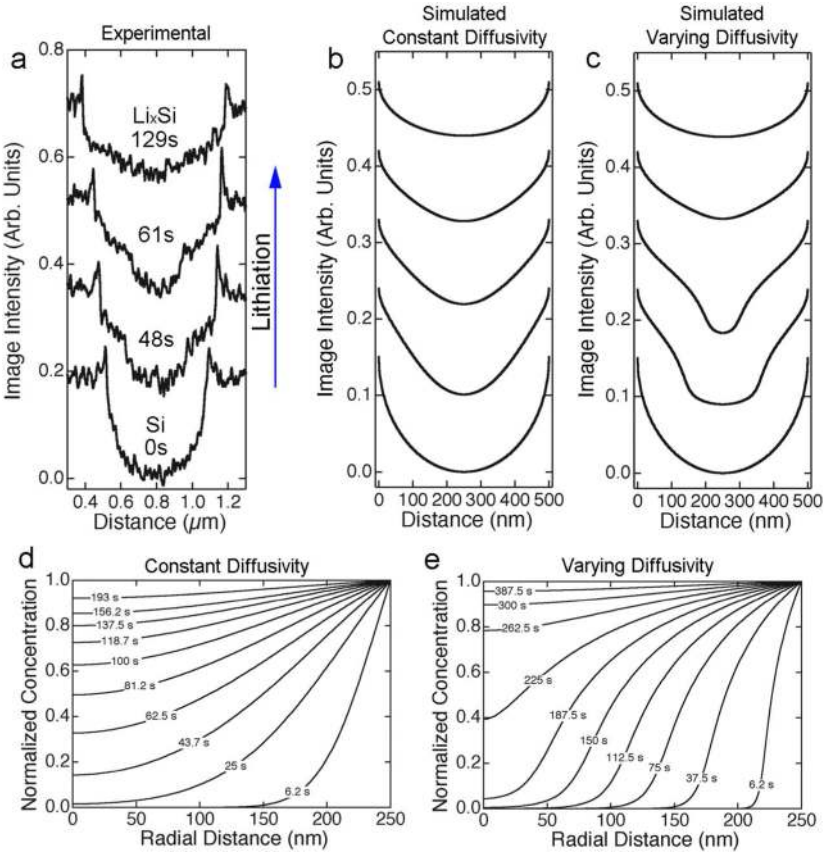

Figure 2. Analyzing the lithiation behavior. (a) Line scans of the image intensity (i.e., image brightness) during lithiation of the sphere from Figure 1. Before lithiation (0 s), the intensity varies smoothly across the sphere due to its varying thickness. During lithiation (48 and 61 s), there is an abrupt change in intensity at the core/shell interface. This indicates a change in concentration since the thickness smoothly varies. The sharp spikes in intensity at the edges of the particle arise because the particle is slightly out of focus. (b,c) Simulated image intensity line scans for comparison to the measured data. The mass–thickness contrast of these profiles is generated by simulating diffusion in a sphere with a diameter of 500 nm; the associated simulated concentration profiles are shown in panels (d) and (e), respectively. Panel (b) shows simulated image intensity profiles at different times assuming a constant diffusivity of 10^{-16} m^2 s^{-1} in the sphere, and the corresponding concentration profiles are shown in (d). Panel (c) shows simulated image intensity profiles assuming concentration-dependent diffusivity with lower diffusivity in Li-poor regions; the corresponding concentration profiles are shown in (e). Concentration-dependent diffusivity results in steeper concentration gradients and image intensity profiles that more closely resemble the experimental profiles. These results clearly show that the sharp contrast observed in the a-Si sphere during lithiation is not due to conventional diffusion; instead, there appears to be some slower rate-limiting process that occurs at the core/shell interface. We simplistically illustrate this here with lower diffusivity in the shell, although this is probably not the physical mechanism at play. See text and Supporting Information for more details regarding simulation methods.

For these experiments, hydrogenated a-Si spheres (approximately 10 atom % hydrogen) were synthesized with methods reported in previous publications.[37–39] The in situ TEM experiments were performed with a specialized dual-probe biasing TEM holder (Nanofactory Instruments AB). One probe consisted of a copper metal rod or Si nanorod array on which a small quantity of a-Si spheres was dispersed, as shown in the schematic in Figure 1a. The other probe was a tungsten rod

dx.doi.org/10.1021/nl3044508 | Nano Lett. XXXX, XXX, XXX–XXX

with a piece of Li metal attached to the tip. The probes were affixed to the TEM holder in an Ar-filled glovebox and transported to the TEM in an airtight container, where the holder was then removed and inserted into the TEM. During this transfer process, the Li was exposed to the air for ~2−5 s, causing a thin layer of oxide to grow on the Li metal; this layer acts as a solid electrolyte in the nanoscale electrochemical cell, as demonstrated in previous studies.[20,24] Inside the TEM, the metallic probes can be spatially manipulated so that the a-Si sphere electrode comes into contact with the Li oxide layer coating the Li electrode, forming an electrochemical cell (Figure 1a). When the a-Si electrode is biased (usually to −3 V in this case), Li ions flow through the solid electrolyte and are reduced at the a-Si, forming a Li−Si alloy phase. Delithiation was performed by using a bias of +3 V. These potentials are larger than those used in actual Li-ion batteries; these values are necessary to drive the Li^+ ions through the solid electrolyte in these experiments. As such, the driving force for reaction is larger here than in conventional batteries, but we do not expect that this will significantly alter reaction mechanisms since previous ex situ and in situ work has shown similar reactions and phase transformations under different experimental conditions.[24,29] For samples where a-Si spheres were dispersed on the sidewalls of Si nanorods, the Si nanorods were contacted to the Li_2O electrolyte layer, and lithiation of both the nanorods and the a-Si spheres occurred.[27] The nanorod array was used because it was experimentally easier to control and visualize the lithiation/delithiation of the spheres with this method. In some experiments in which the nanorod arrays were not used, it was evident that the a-Si spheres broke through the solid electrolyte to directly contact Li metal, which caused chemical lithiation to take place. More details about sphere synthesis and the in situ experiments are in the Supporting Information.

Figure 1b−e shows bright-field TEM images of the lithiation process of a single a-Si sphere (the associated video is in the Supporting Information). In this particular experiment, the sphere is attached to the sidewall of a c-Si nanorod. The diameter of this sphere was 569 nm before lithiation and 792 nm after lithiation, which corresponds to 170% volume expansion. Of 26 spheres that were measured, the total volume expansion varied from 101 to 332% with an average of 204%. This range of volume expansion is probably due to different experimental conditions, such as the quality of electrical contact or variations in the thickness of the solid electrolyte oxide layer, that result in different degrees of lithiation in each sphere. Since the particle in Figure 1 remains amorphous during lithiation, the image contrast of the a-Si evident in Figure 1b−e is governed by the mass (atomic number) and thickness of the specimen. Thicker regions and heavier elements scatter incident electrons more effectively, leading to darker regions in bright-field images. The striking feature from the images is the contrast between the darker core and the lighter shell of the particle midway through lithiation (Figure 1c,d). The core remains approximately spherical because fast surface diffusion of Li results in relatively uniform lithiation from all surfaces.[27] On the basis of electrochemical results, previous work has assumed that the lithiation of a-Si is always a diffusion-controlled single-phase process in which Li and Si form a complete solid solution.[40,41] However, the contrast in the images in Figure 1c,d (which was clearly observed in many samples) seems to indicate that there is a relatively sharp change in Li concentration between the darker Si-rich core and the lighter Li-rich shell; this is not expected from a conventional diffusion-based process. These observations are important because the distribution of Li during lithiation directly affects the stresses in the particle, which can lead to particle fracture; thus, it is important to determine precisely how this reaction proceeds.

Here, we investigate the reaction process in more detail. Figure 2a shows a series of line-scans of the image intensity (image brightness) across the sphere in Figure 1b−e. The intensity scans are averaged to reduce noise; see the Supporting Information for details of the averaging process. The intensity of the pristine Si sphere (Figure 2a, 0 s) varies over the cross section as expected due to its spherical shape. After full lithiation (Figure 2a, 129 s), the image intensity of the lithiated sphere varies in a similar manner but with less contrast between the edges and the middle due to the high concentration of Li (a lighter element than Si) in the sphere. During lithiation (Figure 2a, scans labeled 48 and 61 s), the line scans show relatively sharp contrast (and thus a Li concentration difference) between the darker core and brighter shell regions, and the boundary moves inward as the core disappears. To clearly illustrate the degree to which the observed concentration gradient differs from the conventional diffusion-controlled solid solution case, we have simulated the expected concentration profiles for diffusion in a sphere. To do this, we employ a simple finite-difference simulation to numerically evaluate Fick's second law[42] (see Supporting Information for complete modeling details). For the simulations, the initial concentration of Li is taken to be a constant maximum value at the surface of the sphere and zero everywhere else; this replicates the experimental conditions of fast surface diffusion. Although this simple method is an approximation and does not take into account volume expansion or stress effects on diffusion,[43,44] it serves as a useful comparison to better understand our experimental data. Figure 2d shows expected Li concentration profiles at different times for Li diffusion into a sphere if a constant diffusivity of $D = 10^{-16}$ m^2 s^{-1} is used.[45] In addition, Figure 2b shows simulated TEM image line scans across a spherical particle based on these calculated concentration profiles during lithiation (these simulated line scans include both mass and thickness effects on image contrast). The simulated TEM intensity profiles do not show the sharp dip in intensity in the middle of the particle during lithiation, as observed in the experiments (Figure 2a). For further comparison, Figure 2e shows a different set of concentration profiles generated by simulating diffusion with diffusivity that is strongly concentration-dependent; in this case, the diffusivity is taken to be

$$D = c_{Li}^2 D_{max} + (1 + c_{Li})^2 D_{min}$$

where c_{Li} is the normalized Li concentration and D_{max} and D_{min} are defined to be 10^{-16} and 10^{-17} m^2 s^{-1}, respectively. This functional form results in lower diffusivity in Li-poor regions. As expected, the concentration profiles in Figure 2e are steeper than the constant diffusivity case, resulting in simulated TEM images (Figure 2c) that more closely resemble those obtained in the experiments; the simulated image intensity shows a dip in the core region. However, the contrast between the core and the shell in this simulation is not as sharp as in the experiments. This comparison indicates that the observed behavior is not controlled by conventional diffusion as previously thought; instead, there appears to be a slower process occurring at the interface of the Si-rich core that limits the rate of reaction and

dx.doi.org/10.1021/nl3044508 | Nano Lett. XXXX, XXX, XXX−XXX

causes steeper Li concentration gradients to exist. Although we have modeled this as simply lower diffusivity in Li-poor regions for illustrative purposes, this is probably not the actual physical mechanism at play, as discussed below.

To understand this process, it is helpful to compare to the lithiation of c-Si. The lithiation of c-Si is a two-phase reaction in which the c-Si is consumed to form highly lithiated amorphous Li_xSi.[22,35,46,47] The interface separating the two phases is of nanometer thickness, and the kinetics of the lithiation process has been shown to be limited by the reaction at this interface.[22,27,48,49] Fundamentally, this is because of the kinetic barrier to breaking Si−Si bonds. It has been suggested that the rate of Si−Si bond breakage is higher when there is a higher concentration of Li near the Si−Si bond, which weakens it; this explains why a highly lithiated amorphous phase forms as the c-Si is consumed.[22,35,50] Our data show that a similar phenomenon likely occurs during the lithiation of a-Si; this is not simply a diffusive process, but it also involves Si−Si bond breakage in the amorphous phase. The breaking of the Si−Si bonds is probably a slower process than the diffusion of Li in the Li_xSi phase, which would lead to the kinetics of a-Si lithiation being controlled by the breakup of the Si−Si bonds and the distinct interface observed between the Li-poor and Li-rich phases in our experiments.

Although it appears that the lithiation processes of a-Si and c-Si are more similar than previously thought, there are some key differences. The most noticeable is that fracture has been shown to occur during lithiation of c-Si spheres larger than about 150 nm in diameter and during lithiation of c-Si pillars larger than about 300 nm in diameter,[20,25] but no a-Si spheres were observed to fracture in our experiments (the largest sphere tested was 870 nm in diameter). In c-Si particles, tensile hoop stress develops at the surface due to the two-phase lithiation process: newly created Li_xSi at the core/shell interface pushes out the already-formed Li_xSi, eventually leading to tension at the surface.[20,49] In addition, anisotropic expansion due to the crystallography of c-Si leads to stress intensification and fracture at certain locations.[25] Despite the observation of a two-phase-like lithiation mechanism in a-Si, there are a number of possible reasons why different fracture behavior is observed. First, the concentration of Li in the Li_xSi phase that forms as the Si−Si bonds in the a-Si matrix are broken up is probably lower than that in the c-Si case, which means that there would be less significant volume expansion at the interface and lower stresses. This is supported by our experiments, where in many cases the volume expansion was less than the theoretical 300% after lithiation. Second, the kinetics of bond-breaking in a-Si compared to the kinetics of diffusion in Li_xSi might not be nearly as slow as the kinetics of bond breaking in c-Si relative to diffusion. Depending on the relative rates, this could cause a larger Li concentration gradient in the Li_xSi during a-Si lithiation than during c-Si lithiation (where there is little to no concentration gradient in the Li_xSi), which would result in less tension at the surface in the a-Si case. Third, the thickness of the reaction front is unclear from our experiments; if it is thicker than in the crystalline case, the stresses could be altered. Finally, the stress intensification due to anisotropic expansion of c-Si may result in significantly increased tensile stress values compared to the isotropic a-Si case. Overall, these differences appear to cause a larger critical fracture size for a-Si compared to c-Si even though the lithiation mechanisms are similar. Further understanding the differences in stresses and fracture in amorphous and crystalline Si is an interesting area for future study.

From the TEM images, we can also directly measure the lithiation kinetics of the a-Si spheres. Figure 3 shows a graph of the approximate lithiated thickness as a function of time for a number of different spheres tested. The lithiated thickness is the radial distance measured from the surface to the Si-rich core boundary. Data are shown from spheres that underwent both electrochemical and chemical lithiation (chemical lithiation is where the spheres directly contact lithium metal), and it is evident that chemical lithiation results in faster overall reaction. For all particles, the lithiated thickness increases approximately linearly with time, suggesting reaction front control and not diffusion control of the kinetics.[36] The faster lithiation velocity for chemical lithiation is possibly due to higher concentrations of Li present during these experiments, since it is likely that the reaction kinetics at the Si-rich core is concentration-dependent based on previous discussion.

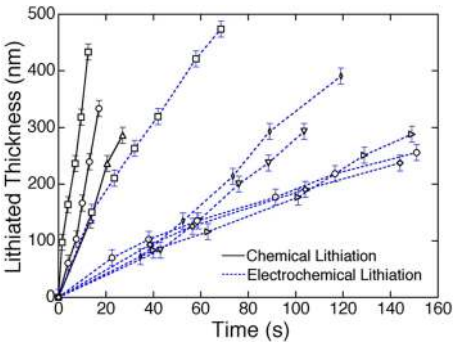

Figure 3. Kinetics of lithiation. This plot shows the lithiated thickness (the distance from the surface to the core/shell interface) as a function of time during lithiation of different a-Si spheres. The lithiated thickness generally increases linearly with time, suggesting that the kinetics of the reaction is controlled by short-range interactions at an interface instead of by diffusion. In addition, spheres that underwent chemical lithiation were lithiated more quickly than those that were electrochemically lithiated. This could be due to concentration-dependent interface reaction kinetics, as discussed in the text.

Interestingly, these results differ significantly from the previously reported case of c-Si nanoparticle lithiation, where even though the reaction is interface-controlled, the interface velocity was observed to slow dramatically with increasing lithiated thickness.[27] The slowing effect was shown to most likely be due to the significant hydrostatic pressure that evolves near the c-Si/Li_xSi interface, which can decrease the driving force for reaction or possibly alter the diffusivity in the vicinity of the reaction front.[27,49] Since no reaction front slowing is evident in the current a-Si lithiation experiments, this indicates that the stress evolution is different in the a-Si spheres; specifically, it suggests that hydrostatic stress is of lower magnitude. This is consistent with the fracture behavior discussed previously.

The delithiation of a-Si spheres was also examined, as shown in Figure 4. As mentioned before, most of the spheres remained amorphous after lithiation, which is different than in situ TEM results of c-Si lithiation where the formation of the crystalline $Li_{15}Si_4$ phase is commonly observed.[26,36] In a few instances, however, a lithiated crystalline phase was seen (presumably $Li_{15}Si_4$), but the patterns were not indexed due to insufficient diffraction spots. In any case, Figure 4 shows the lithiation and

dx.doi.org/10.1021/nl3044508 | Nano Lett. XXXX, XXX, XXX−XXX

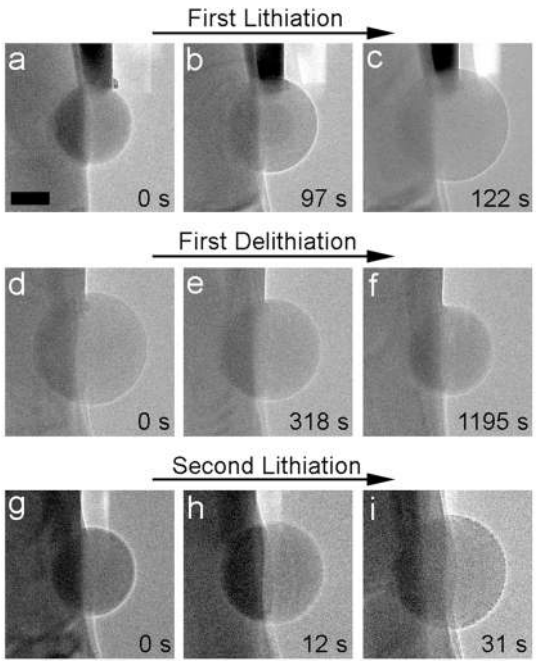

Figure 4. Cycling of an a-Si sphere. (a–c) First lithiation. In (b), the sharp mass–thickness contrast in the partially lithiated sphere reveals characteristic two-phase behavior. (d–f) First delithiation. No phase front is visible in the images. (g–i) Second lithiation. Again, no phase front is visible. The scale bar is 200 nm.

delithiation process of a sphere that remains amorphous during cycling. During the first lithiation (Figure 4a–c), the concentration boundary is evident in the partially lithiated state (Figure 4b). During the first delithiation (Figure 4d–f), however, it appears that the reaction occurs via a single-phase mechanism since no concentration boundary is visible when the sphere is partially delithiated (Figure 4e). This is consistent with our previous discussion since Si–Si bond breaking does not occur during delithiation, so Li diffusion in the partially lithiated phase dominates the reaction. It is interesting to note that during single-phase delithiation, hoop tension is expected to develop at the surface due to lower Li concentrations there, but this stress is apparently not significant enough to cause the particle in Figure 4 to fracture.

Figure 4g-i shows the same sphere during the second lithiation process. The results are different than the first lithiation; here, no concentration boundary is visible and the reaction process appears to be single-phase. This indicates that the initial lithiation of the a-Si material is different than subsequent lithiation cycles, which is probably why previous in situ studies on c-Si lithiation/delithiation have not observed or commented on the two-phase lithiation process during cycling of amorphous material. Differences in the first and subsequent lithiation processes may be caused by a number of factors, including (1) the possible trapping of Li in the a-Si matrix after the first delithiation[51] or (2) structural changes after the first delithiation that cause extra Si dangling bonds to be present in the a-Si.[52] These features could contribute to the observed single-phase lithiation mechanism after the first cycle since Si–Si bonding in the a-Si matrix would be less prevalent. It is important to note that before the second lithiation in Figure 4c, the delithiated particle was 25% larger than the initial particle volume, indicating either that Li remained in the sphere or that the delithiated phase was of lower density; this could have contributed to the single-phase mechanism observed. To summarize these results and to present a full picture of the general lithiation/delithiation process for Si, Figure 5 schematically shows the first lithiation and cycling behavior of a-Si compared to c-Si.

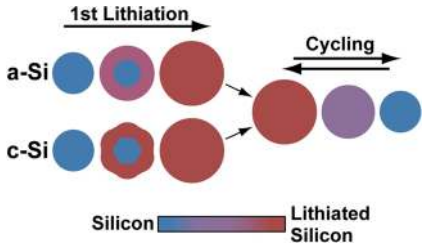

Figure 5. Summary of the first lithiation and subsequent cycling of a-Si and c-Si. This figure is color-coded by Li content with blue as pure Si and red as the fully lithiated phase. The first lithiation for both materials is characterized by a two-phase reaction, but there are important differences. The c-Si particle undergoes anisotropic lithiation and volume expansion, leading to a faceted Si core; in addition, the lithiated phase is very nearly fully lithiated. The a-Si particle is lithiated isotropically, and the concentration of Li in the lithiated phase is probably lower than the crystalline case and may vary with position. Additionally, the reaction of a-Si proceeds approximately linearly in time, but significant reaction front slowing occurs during lithiation of c-Si. After the first lithiation, delithiation and subsequent lithiation cycles proceed via a single-phase mechanism for both materials, assuming the lithiated phase remains amorphous (if the crystalline $Li_{15}Si_4$ phase forms at full lithiation, then a two-phase reaction will occur upon delithiation, as previously shown[55] but not discussed here).

Previous electrochemical cycling data also give some indication that different chemical processes occur during the first and subsequent lithiation cycles in a-Si, similar to our observations. In many reports, the first lithiation voltage profile of a-Si anodes occurs at slightly lower voltages and is sometimes somewhat flatter than subsequent lithiation profiles.[10,51,53,54] These differences are generally consistent with the proposed reaction process here, and they indicate that the chemical processes occurring during the first and subsequent reactions could be different. The flatter first lithiation voltage (at least for part of the capacity range) suggests a two-phase-like reaction, while the higher sloping voltage of subsequent cycles indicates a one-phase reaction. In future studies, it would be interesting to determine the atomic-scale mechanisms responsible for the differences in reaction behavior on the first and subsequent lithiation cycles. In addition, it would also be useful to establish whether the lithiation rate has any effect on the two-phase reaction. In this study, the large biases that are used result in relatively fast lithiation; it is possible that with slower lithiation rates the two-phase mechanism may be less pronounced.

In conclusion, our in situ TEM results of the Li reaction with a-Si spheres have revealed a variety of interesting aspects of this technologically important solid-state reaction. The sharp concentration gradient evident during the first lithiation suggests a two-phase lithiation mechanism that has not previously been observed. This discovery is important, since the stress evolution and fracture behavior are strongly influenced by the lithiation mechanism.[20,25] Although these observations indicate that the first lithiation of a-Si is more similar to c-Si than previously thought; there are some

dx.doi.org/10.1021/nl3044508 | Nano Lett. XXXX, XXX, XXX–XXX

significant differences. In particular, the critical size for fracture is larger for a-Si spheres, and the lithiation reaction velocity is approximately constant and does not slow as in the crystalline case, which suggests different stress evolution during lithiation. These results imply that a-Si undergoes more manageable physical transformations than c-Si during the first cycle, which may make it a more desirable active material. Overall, this study reveals new information about the fundamental nature of the lithiation of Si with the hope that it will assist in the design of better-performing battery materials.

■ ASSOCIATED CONTENT

Supporting Information

Additional information, figures, and movies. This material is available free of charge via the Internet at http://pubs.acs.org.

■ AUTHOR INFORMATION

Corresponding Author

*E-mail: yicui@stanford.edu. Phone: 650-723-4613. Fax: 650-725-4034.

Notes

The authors declare no competing financial interest.

■ ACKNOWLEDGMENTS

M.T.M. acknowledges support from the Chevron Stanford Graduate Fellowship and the National Science Foundation Graduate Fellowship. This work is supported by the U.S. Department of Energy, Office of Basic Energy Sciences, Division of Materials Sciences and Engineering under Contract No. DE-AC02-76SF00515 through the SLAC National Accelerator Laboratory LDRD project and the Assistant Secretary for Energy efficiency and Renewable Energy, Office of Vehicle Technologies of the U.S. Department of Energy under Contract No. DE-AC02-05CH11231, Subcontract No. 6951379 under the Batteries for Advanced Transportation Technologies (BATT) Program. The in situ TEM work was conducted in the William R. Wiley Environmental Molecular Sciences Laboratory (EMSL), a national scientific user facility sponsored by DOE's Office of Biological and Environmental Research and located at PNNL. PNNL is operated by Battelle for the DOE under Contract DE-AC05-76RLO1830. C.M.W. thanks the support of the chemical imaging initiative of PNNL. W.D.N. gratefully acknowledges support of the Office of Science, Office of Basic Energy Sciences, of the U.S. Department of Energy under contract no. DE-FG02-04ER46163. The synthesis of a-Si spheres by J.T.H. and B.A.K. was supported as part of the program "Understanding Charge Separation and Transfer at Interfaces in Energy Materials (EFRC: CST)", an Energy Frontier Research Center funded by the U.S. Department of Energy Office of Science, Office of Basic Energy Sciences, under Award No. DE-SC0001091.

■ REFERENCES

(1) Armand, M.; Tarascon, J. M. *Nature* **2008**, *451* (7179), 652−657.
(2) Whittingham, M. S. *MRS Bull.* **2008**, *33* (4), 411−419.
(3) Marom, R.; Amalraj, S. F.; Leifer, N.; Jacob, D.; Aurbach, D. *J. Mater. Chem.* **2011**, *21* (27), 9938−9954.
(4) Hayner, C. M.; Zhao, X.; Kung, H. H. *Ann. Rev. Chem. Biomol. Eng.* **2012**, *3* (1), 445−471.
(5) Wu, H.; Cui, Y. *Nano Today* **2012**, *7* (5), 414−429.
(6) Kasavajjula, U.; Wang, C. S.; Appleby, A. J. *J. Power Sources* **2007**, *163* (2), 1003−1039.
(7) Chan, C. K.; Peng, H. L.; Liu, G.; McIlwrath, K.; Zhang, X. F.; Huggins, R. A.; Cui, Y. *Nat. Nanotechnol.* **2008**, *3* (1), 31−35.
(8) Wu, H.; Chan, G.; Choi, J. W.; Ryu, I.; Yao, Y.; McDowell, M. T.; Lee, S. W.; Jackson, A.; Yang, Y.; Hu, L.; Cui, Y. *Nat. Nanotechnol.* **2012**, *7* (5), 310−315.
(9) Yao, Y.; McDowell, M. T.; Ryu, I.; Wu, H.; Liu, N. A.; Hu, L. B.; Nix, W. D.; Cui, Y. *Nano Lett.* **2011**, *11* (7), 2949−2954.
(10) Cui, L.-F.; Yang, Y.; Hsu, C.-M.; Cui, Y. *Nano Lett.* **2009**, *9* (9), 3370−3374.
(11) Kovalenko, I.; Zdyrko, B.; Magasinski, A.; Hertzberg, B.; Milicev, Z.; Burtovyy, R.; Luzinov, I.; Yushin, G. *Science* **2011**, *334* (6052), 75−79.
(12) Hertzberg, B.; Alexeev, A.; Yushin, G. *J. Am. Chem. Soc.* **2010**, *132* (25), 8548.
(13) Magasinski, A.; Dixon, P.; Hertzberg, B.; Kvit, A.; Ayala, J.; Yushin, G. *Nat. Mater.* **2010**, *9* (4), 353−358.
(14) Hwang, T. H.; Lee, Y. M.; Kong, B.-S.; Seo, J.-S.; Choi, J. W. *Nano Lett.* **2011**, *12* (2), 802−807.
(15) Kim, H.; Seo, M.; Park, M. H.; Cho, J. *Angew. Chem., Int. Ed.* **2010**, *49* (12), 2146−2149.
(16) Song, T.; Xia, J. L.; Lee, J. H.; Lee, D. H.; Kwon, M. S.; Choi, J. M.; Wu, J.; Doo, S. K.; Chang, H.; Il Park, W.; Zang, D. S.; Kim, H.; Huang, Y. G.; Hwang, K. C.; Rogers, J. A.; Paik, U. *Nano Lett.* **2010**, *10* (5), 1710−1716.
(17) Esmanski, A.; Ozin, G. A. *Adv. Funct. Mater.* **2009**, *19* (12), 1999−2010.
(18) Liu, N.; Wu, H.; McDowell, M. T.; Yao, Y.; Wang, C.; Cui, Y. *Nano Lett.* **2012**, *12* (6), 3315−3321.
(19) Li, X.; Meduri, P.; Chen, X.; Qi, W.; Engelhard, M. H.; Xu, W.; Ding, F.; Xiao, J.; Wang, W.; Wang, C.; Zhang, J.-G.; Liu, J. *J. Mater. Chem.* **2012**, *22* (22), 11014−11017.
(20) Liu, X. H.; Zhong, L.; Huang, S.; Mao, S. X.; Zhu, T.; Huang, J. Y. *ACS Nano* **2012**, *6* (2), 1522−1531.
(21) Liu, X. H.; Liu, Y.; Kushima, A.; Zhang, S.; Zhu, T.; Li, J.; Huang, J. Y. *Adv. Energy Mat.* **2012**, *2* (7), 722−741.
(22) Liu, X. H.; Wang, J. W.; Huang, S.; Fan, F.; Huang, X.; Liu, Y.; Krylyuk, S.; Yoo, J.; Dayeh, S. A.; Davydov, A. V.; Mao, S. X.; Picraux, S. T.; Zhang, S.; Li, J.; Zhu, T.; Huang, J. Y. *Nat. Nanotechnol.* **2012**, *7* (11), 749−756.
(23) Kushima, A.; Huang, J. Y.; Li, J. *ACS Nano* **2012**, *6* (11), 9425−9432.
(24) Liu, X. H.; Zheng, H.; Zhong, L.; Huan, S.; Karki, K.; Zhang, L. Q.; Liu, Y.; Kushima, A.; Liang, W. T.; Wang, J. W.; Cho, J. H.; Epstein, E.; Dayeh, S. A.; Picraux, S. T.; Zhu, T.; Li, J.; Sullivan, J. P.; Cumings, J.; Wang, C. S.; Mao, S. X.; Ye, Z. Z.; Zhang, S. L.; Huang, J. Y. *Nano Lett.* **2011**, *11* (8), 3312−3318.
(25) Lee, S. W.; McDowell, M. T.; Berla, L. A.; Nix, W. D.; Cui, Y. *Proc. Natl. Acad. Sci. U.S.A.* **2012**, *109* (11), 4080−4085.
(26) McDowell, M. T.; Lee, S. W.; Wang, C.; Cui, Y. *Nano Energy* **2012**, *1* (3), 401−410.
(27) McDowell, M. T.; Ryu, I.; Lee, S. W.; Wang, C.; Nix, W. D.; Cui, Y. *Adv. Mater.* **2012**, *24* (45), 6034−6041.
(28) McDowell, M. T.; Cui, Y. *Adv. Energy Mater.* **2011**, *1* (5), 894−900.
(29) Lee, S. W.; McDowell, M. T.; Choi, J. W.; Cui, Y. *Nano Lett.* **2011**, *11* (7), 3034−3039.
(30) Karki, K.; Epstein, E.; Cho, J.-H.; Jia, Z.; Li, T.; Picraux, S. T.; Wang, C.; Cumings, J. *Nano Lett.* **2012**, *12* (3), 1392−1397.
(31) Wang, C.-M.; Li, X.; Wang, Z.; Xu, W.; Liu, J.; Gao, F.; Kovarik, L.; Zhang, J.-G.; Howe, J.; Burton, D. J.; Liu, Z.; Xiao, X.; Thevuthasan, S.; Baer, D. R. *Nano Lett.* **2012**, *12* (3), 1624−1632.
(32) Gu, M.; Li, Y.; Li, X.; Hu, S.; Zhang, X.; Xu, W.; Thevuthasan, S.; Baer, D. R.; Zhang, J.-G.; Liu, J.; Wang, C. *ACS Nano* **2012**, *6* (9), 8439−8447.
(33) Ghassemi, H.; Au, M.; Chen, N.; Heiden, P. A.; Yassar, R. S. *ACS Nano* **2011**, *5* (10), 7805−7811.
(34) Misra, S.; Liu, N.; Nelson, J.; Hong, S. S.; Cui, Y.; Toney, M. F. *ACS Nano* **2012**, *6* (6), 5465−5473.

(35) Key, B.; Bhattacharyya, R.; Morcrette, M.; Seznec, V.; Tarascon, J. M.; Grey, C. P. *J. Am. Chem. Soc.* **2009**, *131* (26), 9239−9249.
(36) Liu, X. H.; Zhang, L. Q.; Zhong, L.; Liu, Y.; Zheng, H.; Wang, J. W.; Cho, J.-H.; Dayeh, S. A.; Picraux, S. T.; Sullivan, J. P.; Mao, S. X.; Ye, Z. Z.; Huang, J. Y. *Nano Lett.* **2011**, *11* (6), 2251−2258.
(37) Harris, J. T.; Hueso, J. L.; Korgel, B. A. *Chem. Mater.* **2010**, *22* (23), 6378−6383.
(38) Murugesan, S.; Harris, J. T.; Korgel, B. A.; Stevenson, K. J. *Chem. Mater.* **2012**, *24* (7), 1306−1315.
(39) Pell, L. E.; Schricker, A. D.; Mikulec, F. V.; Korgel, B. A. *Langmuir* **2004**, *20* (16), 6546−6548.
(40) Zhao, K. J.; Pharr, M.; Cai, S. Q.; Vlassak, J. J.; Suo, Z. G. *J. Am. Ceram. Soc.* **2011**, *94*, S226−S235.
(41) Cheng, Y. T.; Verbrugge, M. W. *J. Power Sources* **2009**, *190* (2), 453−460.
(42) Crank, J. *The Mathematics of Diffusion*, 2nd ed.; Oxford University Press: Walton Street, Oxford, 1975.
(43) Grantab, R.; Shenoy, V. B. *J. Electrochem. Soc.* **2012**, *159* (5), A584−A591.
(44) Ryu, I.; Choi, J. W.; Cui, Y.; Nix, W. D. *J. Mech. Phys. Solids* **2011**, *59* (9), 1717−1730.
(45) Ding, N.; Xu, J.; Yao, Y. X.; Wegner, G.; Fang, X.; Chen, C. H.; Lieberwirth, I. *Solid State Ionics* **2009**, *180* (2−3), 222−225.
(46) Chon, M. J.; Sethuraman, V. A.; McCormick, A.; Srinivasan, V.; Guduru, P. R. *Phys. Rev. Lett.* **2011**, *107* (4), 045503.
(47) Limthongkul, P.; Jang, Y. I.; Dudney, N. J.; Chiang, Y. M. *Acta Mater.* **2003**, *51* (4), 1103−1113.
(48) Pharr, M.; Zhao, K.; Wang, X.; Suo, Z.; Vlassak, J. J. *Nano Lett.* **2012**, *12* (9), 5039−5047.
(49) Zhao, K. J.; Pharr, M.; Wan, Q.; Wang, W. L.; Kaxiras, E.; Vlassak, J. J.; Suo, Z. G. *J. Electrochem. Soc.* **2012**, *159* (3), A238−A243.
(50) Tu, K. N. *Appl. Phys. Lett.* **1975**, *27* (4), 221−224.
(51) Baranchugov, V.; Markevich, E.; Pollak, E.; Salitra, G.; Aurbach, D. *Electrochem. Commun.* **2007**, *9* (4), 796−800.
(52) Key, B.; Morcrette, M.; Tarascon, J.-M.; Grey, C. P. *J. Am. Chem. Soc.* **2010**, *133* (3), 503−512.
(53) Maranchi, J. P.; Hepp, A. F.; Kumta, P. N. *Electrochem. Solid-State Lett.* **2003**, *6* (9), A198−A201.
(54) Jung, H.; Park, M.; Yoon, Y.-G.; Kim, G.-B.; Joo, S.-K. *J. Power Sources* **2003**, *115* (2), 346−351.
(55) Obrovac, M. N.; Christensen, L. *Electrochem. Solid-State Lett.* **2004**, *7* (5), A93−A96.